Int. J. Heat Mass Transfer. Vol. 36, No. 10, pp. 2623–2634, 1993
Printed in Great Britain

0017–9310/93 $6.00 + 0.00

Mass flow sensing with heat waves: the effect of gas pressure

DAVID K. LAMBERT
Physics Department, General Motors Research and Environmental Staff, Warren, MI 48090–9055, U.S.A.

(*Received* 28 *May* 1992 *and in final form* 16 *October* 1992)

Abstract—Two conceptual examples are given of mass flow sensors based on heat waves that have *exact* gas pressure self-compensation in uniform flow: one with a plane heat source through which the flow passes, and one with a line source. Both sensors ratio the heat wave amplitudes detected at equal distances upstream and downstream from the source. Heat wave fronts from either source expand symmetrically upstream and downstream. An automotive air flow sensor based on heat waves is also described and modeled. It is a microelectronic device on silicon. This sensor is approximately, but not exactly, self-compensated for pressure change.

1. INTRODUCTION

THE ABILITY to measure the mass flow of a gas, independent of pressure, is essential in some applications. One way to measure mass flow, with self-compensation for gas pressure, is by convective heat transfer from a solid to the flowing gas. This paper shows that heat waves can also be used to measure the mass flow of a gas, with self-compensation for pressure change.

An example of a mass flow sensor based on heat waves is shown schematically in Fig. 1(a). It compares the decay rate of heat waves moving upstream with that of heat waves moving downstream. The amplitude of temperature oscillation is measured at two points—equal distances upstream and downstream from a line source of oscillating heat. The ratio of the two amplitudes is dependent on the flow rate. The sensor's output also identifies the flow direction.

Heat waves decay exponentially with distance in the upstream direction. As a result, for a sensor like that in Fig. 1(a) to detect enough upstream signal to operate properly, the propagation length must be comparable to the thermal decay length—the sensor must be compact in the streamwise direction.

The present work grew out of effort to develop an air flow sensor based on heat wave propagation [1] to sense mass air flow into the automobile engine. Experiments indicate that the sensor is approximately self-compensated for pressure change. To understand why, a computational model for the automotive air flow sensor was developed. The model is presented here and used to investigate the effect of pressure change on the sensor's response at constant mass air flow.

The automotive sensor is different from the ideal sensor in Fig. 1(a) in that the source and detectors of heat waves are all on a solid surface, not in the free stream. A solid substrate is necessary in the automotive application. A sensor with a substrate is very robust. The automotive sensor is a microelectronic device on a silicon substrate. The sensor actually responds only to flow very near the surface—in the boundary layer. Air flow into the engine is turbulent, but flow in the boundary layer over the sensor is laminar. The effect of main stream turbulence on the sensor's output is primarily to cause noise—the limiting flow velocity at the outer edge of the boundary layer varies as a function of time. In the present analysis the velocity in the boundary layer is assumed to be steady.

Microelectronic flow sensors based on steady-state heat transfer have also been developed [2–13]. They compare temperature between two locations. With a constant heat input, the average temperature difference is a function of mass air flow.

An air flow sensor that closely approximates the sensor, in Fig. 1(a) was developed earlier by Kielbasa and co-workers [14–16]. Kielbasa's sensor uses closely spaced hot wires as source and detectors of heat waves. Although an analytical model of Kielbasa's sensor has been published [15, 16], it has not been recognized as a mass air flow sensor. The published model does imply, however, that Kielbasa's sensor is self-compensated for pressure change.

It is well known that flow *velocity* can be measured with heat waves [14–24] or pulses [25–34]. In uniform steady flow, the centroid of a pulse of heat (or other diffusing species) drifts downstream at the mean flow velocity. Even in situations with shear, as in laminar flow through a tube, if a diffusive tracer (like heat) is introduced as a pulse and the tracer does not interact with the walls, the centroid of the pulse eventually moves downstream at the mean flow velocity [33–39]. It is thus surprising that heat waves can also be used to measure mass flow.

The present flow measurement technique involves thermal diffusion in the upstream direction. Although

NOMENCLATURE

a width of heat source, Fig. 2(b)
A cross-sectional area of duct
b complex valued quantity of dimension $1/L$, equation (9)
c_p heat capacity at constant pressure
C prefactor for heat wave amplitude
d thickness of polyimide layer, Fig. 2(b)
$f'(\eta)$ normalized velocity in the boundary layer
$G(\mathbf{r}', \mathbf{r})$ Green's function, equation (D3)
$H(\mathbf{r})$ spatially distributed heat source
$H_1(\mathbf{r})$ effect of flow as a distributed heat source, equation (D2)
i unit pure imaginary number
I_m mass flow through a duct
K_0 associated Bessel function of zero order
L_0 length used to define Pe in equation (1)
m complex valued quantity of dimension $1/L$
M_A, M_B, M_C, M_D intermediate quantities used in equation (C4)
p pressure
Pe Peclet number, equation (1)
Q dimensionless effect of p on measured I_m, equation (23)
r distance from source
$\mathbf{r}$ position vector
R sensor's response
s quantity of dimension $1/L$ used in Fourier transforms
t time
$T(\mathbf{r}, t)$ time-dependent temperature distribution
$T(\mathbf{r}, \omega)$ complex amplitude of oscillatory temperature distribution
T_a exact temperature distribution with no flow, source width a
T_L exact temperature distribution with slug flow, line heat source
$T_0(\mathbf{r})$ steady part of temperature distribution
$T_1(\mathbf{r}, \omega)$ ε term in perturbation series for temperature distribution
$T_{11}(\mathbf{r}, \omega)$ ε^2 term in perturbation series for temperature distribution
T_c temperature distribution perturbed by flow, equation (18)
$u(y)$ flow velocity distribution
$\bar{u}$ flow velocity averaged over duct cross-section
u_0 phase velocity in motionless fluid, equation (12)
u_∞ flow velocity outside of the boundary layer
u_p phase velocity, equation (11)
W amplitude of oscillatory part of dissipated power
W_0 steady part of dissipated power
x coordinate in the direction of flow
$\hat{\mathbf{x}}$ unit vector in the flow direction
y coordinate normal to the source and the flow.

Greek symbols

α thermal diffusivity, equation (2)
β flow velocity in slug flow model, equation (20)
δ delta function of distribution theory
Δ finite-difference—as in equations (21) and (23)
ε scale factor used in perturbation theory
η dimensionless distance y
κ thermal conductivity
λ wavelength of heat wave in still fluid, equation (4)
Λ effect of flow at y on $T(x, 0, \omega)$, equation (D7)
ν kinematic viscosity
ξ complex valued quantity of dimension $1/L$, equation (A1)
ρ density
τ time delay of phase relative to source, equation (16)
ϕ phase
χ ratio of heat wave amplitudes, equation (22)
ω angular frequency, in rad s^{-1}.

Superscripts and subscripts

$\tilde{}$ Fourier transformed quantity with respect to x
$+$ defined on positive coordinate values
$-$ defined on negative coordinate values
1 quantity for air
2 quantity for polyimide
3 quantity for silicon.

the centroid of a heat pulse never moves upstream, a localized pulse of heat does cause a subsequent temperature rise upstream, from diffusion.

There have been previous theoretical studies concerned with streamwise diffusion of heat waves or pulses in a flowing fluid. Neuringer [40] obtained the transient solution for a pulsed line source in shear flow. In connection with Kielbasa's device, a solution was obtained [15, 16] for the heat waves from a line source in uniform steady flow. With slug flow (uni-

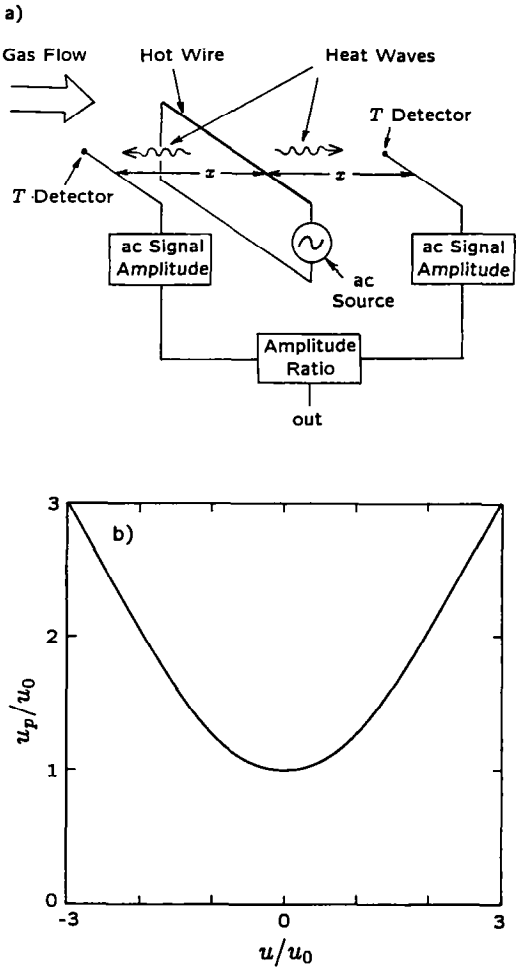

FIG. 1. (a) Schematic diagram of a sensor that uses heat waves from a line source to measure the direction and mass flow of a gas. Temperature detectors are equally spaced upstream and downstream from the source. The amplitude of the ac component of each signal is determined. The ratio of the two amplitudes is the sensor's output. (b) Phase velocity u_p of heat waves from a plane source, in fluid moving uniformly at velocity u normal to the source. The phase velocity u_0 in still fluid is used for normalization. In air, at 160 Hz, $u_0 = 21.2$ cm s^{-1}.

form velocity even at the interface) over a flat plate with an edge, solutions have also been obtained [41, 42] for the temperature transient caused by a jump in dissipated power.

The present paper is organized as follows. Section 2 discusses why steady state heat transfer from a solid to a gas—with pressure and velocity as variables—is a function only of the mass flow of the gas, and why flow sensing by heat waves is fundamentally different. Sections 3 and 4 show that two idealized sensors based on heat waves measure the mass flow of a gas. The first uses a plane source; the second, a line source (like Kielbasa's device). Section 5 develops a model for the automotive air flow sensor. Part of the model is a perturbation solution that is exact in the limit of low flow. A solution is also obtained for the artificial situation of slug flow; it is mathematically exact at all flow velocities. The slug flow solution is used to check the perturbation solution. Section 6 combines the slug flow solution with the perturbation solution and with a realistic boundary layer, in a computational model of the automotive sensor's flow response. The computational model is used to investigate the effect of pressure change on the automotive sensor's flow response. Finally, the results are summarized.

2. BACKGROUND

Steady-state convective heat transfer to a gas is self-compensated for pressure change because of dynamic similarity, together with the pressure independence of the thermal conductivity κ and viscosity of an ideal gas at constant ambient temperature [43]. Self-compensation for pressure change breaks down if the flow velocity is low enough for natural convection to be important, if the flow velocity is large enough to be comparable to the speed of sound, or if temperature differences are large.

Various flow sensors based on steady-state convective heat exchange have been developed [44, 45]. For example, some hot wire sensors use feedback to maintain a constant temperature difference relative to the ambient. Sensor output is proportional to convective heat loss. Other hot wire sensors operate with a constant current and detect flow as a change in resistance. With constant ambient temperature, the output of either type of sensor is determined by the Peclet number

$$Pe = \frac{u_\infty L_0}{\alpha}. \tag{1}$$

Here u_∞ is the flow velocity outside the boundary layer, α is the thermal diffusivity, and L_0 is a characteristic dimension. By definition

$$\alpha = \frac{\kappa}{\rho c_p} \tag{2}$$

where ρ is the density and c_p is the heat capacity at constant pressure p. Hence, Pe is a function of ρu_∞. In a duct with cross-sectional area A the mass flow

$$I_m = A\rho\bar{u}. \tag{3}$$

Here $\bar{u}$ is the velocity averaged over the duct cross section. Both $\rho\bar{u}$ and ρu_∞ are functions of the Reynolds number, independent of p. Consequently, Pe is a function of I_m alone, independent of any other change, as long as the change does not affect c_p/κ or the thermal properties of the solid. Changing p does not affect any of these quantities, so a hot wire sensor responds to I_m independent of p.

Some flow sensors based on steady-state convective heat exchange are too large to be described by a u_∞ at a single point. The sensor's output, however, is still determined by the heat transfer at the surface. At each point on the surface the heat transfer is a function of

Table 1. Thermal conductivity κ and thermal diffusivity α of air, silicon, and the polyimide used in the automotive air flow sensor. For the meaning of the other parameters see Fig. 2(b). The present values of κ, α, and ν are for 298 K and $p = 100$ kPa. For air, κ_1 is to good approximation independent of p, but α_1 and ν vary as p^{-1}

Parameter	Value	Units	Description
κ_1	2.60×10^{-4}	W(cm K)$^{-1}$	Air thermal conductivity [47]
κ_2	2.13×10^{-3}	W(cm K)$^{-1}$	Polyimide thermal conductivity [51]
κ_3	1.49	W(cm K)$^{-1}$	Silicon thermal conductivity [49]
α_1	2.24×10^{-1}	cm^2 s^{-1}	Air thermal diffusivity [47, 48]
α_2	1.57×10^{-3}	cm^2 s^{-1}	Polyimide thermal diffusivity [51]
α_3	0.89	cm^2 s^{-1}	Silicon thermal diffusivity [50]
ν	1.60×10^{-1}	cm^2 s^{-1}	Air kinematic viscosity [48, 55]
a	59	μm	Width of heat source
d	14.5	μm	Polyimide thickness
x	71	μm	Distance from center of heat source to detector
x_0	4.1	mm	Distance from leading edge to heat source
$\omega/2\pi$	160	Hz	Frequency of temperature oscillation

$\rho\bar{u}$. Consequently, the output of the sensor is self-compensated to respond to I_m independent of p. Fundamentally, sensors based on steady-state heat exchange are self-compensated for p because the local Pe is a function only of local mass flow.

Heat waves involve a decay length in addition to Pe. In a still fluid, heat waves decay with distance x away from a source as $\exp(-x/\lambda)$ where

$$\lambda = \sqrt{(2\alpha/\omega)}. \tag{4}$$

Here ω is the angular frequency of the source. The α of air at 298 K and 100 kPa is given in Table 1. For a source in air, oscillating at 100 Hz, $\lambda = 267$ μm. It is evident from equations (2) and (4) that λ changes with p. As a consequence, the oscillating temperature does depend on p. Surprisingly, it is still possible for the output of a flow sensor based on an oscillating source to depend only on I_m, independent of p.

In the present paper, the time-dependent temperature increase (heat wave) produced by an oscillating heat source is $T(\mathbf{r}, t)$. The source is assumed to vary as $W_0 + W\cos(\omega t)$. The Fourier transform of $T(\mathbf{r}, t)$ is time independent but complex valued

$$T(\mathbf{r}, t) = T_0(\mathbf{r}) + \mathrm{Re}[T(\mathbf{r}, \omega)\exp(\mathrm{i}\omega t)]. \tag{5}$$

Heat waves are completely described by $T(\mathbf{r}, \omega)$. The phase at $\mathbf{r}$ relative to the source is $\arg[T(\mathbf{r}, \omega)]$.

One way to check $T(\mathbf{r}, \omega)$ is to consider the limit as $\omega \to 0$. It should approach the steady temperature rise produced by the corresponding steady heat source.

3. PLANE HEAT WAVE SOURCE

This section considers a simple situation that contains the essential aspects of flow measurement with heat waves. The source of oscillating heat is a plane through which a gas flows with velocity u in the normal direction. Heat waves move upstream and downstream away from the plane.

By symmetry $T(\mathbf{r}, \omega)$ depends only on the normal coordinate x. It obeys the equation

$$\mathrm{i}\omega T = \alpha\frac{\partial^2 T}{\partial x^2} - u\frac{\partial T}{\partial x}. \tag{6}$$

The boundary conditions are that $T(x, t)$ is continuous and that the net heat flux away from the interface (per unit area) is equal to the dissipated power: $W_0 + W\cos(\omega t)$. There are corresponding boundary conditions for $T(x, \omega)$. Let T_+ and T_- be $T(x, \omega)$ for $x \geq 0$ and $x \leq 0$, respectively. Then at

$$x = 0: \quad T_+ = T_-, \quad -\kappa\frac{\partial T_+}{\partial x} + \kappa\frac{\partial T_-}{\partial x} = W. \tag{7}$$

The solution to equations (6) and (7) is derived in Appendix A. For $u \geq 0$ the solution is

$$T(x, \omega) = \frac{W}{2\kappa b}\exp\left(\frac{Pe\,x}{2L_0} - |x|b\right) \tag{8}$$

where L_0 is the length used to define Pe and

$$b = \sqrt{\left(\left(\frac{u}{2\alpha}\right)^2 + \mathrm{i}\frac{\omega}{\alpha}\right)}. \tag{9}$$

One way to check this solution is to examine the limit as $\omega \to 0$. Physically, this corresponds to the steady-state temperature in fluid that flows through a very thin heat exchanger. As expected, the temperature rise caused by the source decays exponentially with distance in the upstream direction, and is constant downstream: $T_0 = W_0/(u\rho c_p)$.

At finite ω, $T(x, \omega)$ is an exponentially damped wave that decays as it moves away from the source both in the upstream and downstream directions. There is symmetry between $T(x, \omega)$ and $T(-x, \omega)$ so that

$$\frac{T(x, \omega)}{T(-x, \omega)} = \exp(Pe\,x/L_0). \tag{10}$$

With x fixed, the ratio is a function only of Pe. Since Pe is a function only of mass air flow, independent of p, a sensor that measures the ratio is a mass air flow sensor and is exactly compensated for change in p.

A sensor that compares the arrival time of heat waves

upstream and downstream from a plane source cannot use the same symmetry. Since the ratio in equation (10) is real, the phase ϕ of $T(x, \omega)$ is the same at x and $-x$. The phase velocity u_p is the speed at which a phase front moves away from the source. Since ϕ is the same at x and at $-x$, the wave moves at the same phase velocity in both the upstream and downstream directions. *The phase velocity of a thermal wave in a moving fluid is not simply the vector sum of u and the phase velocity in still fluid.* Explicitly, for $x > 0$,

$$u_p = \omega\left(\frac{d\phi}{dx}\right)^{-1} = \omega/\mathrm{Im}\, b. \tag{11}$$

In this one-dimensional situation, u_p is independent of distance from the source. A plot of u_p/u_0 vs u/u_0 is given in Fig. 1(b), where

$$u_0 = \sqrt{(2\alpha\omega)} \tag{12}$$

is u_p in the motionless fluid. Note that u_p asymptotically approaches u in the downstream direction and $-u$ in the upstream direction. Clearly, the u_p of heat waves from a plane source in air is not compensated for change in p.

4. LINE HEAT WAVE SOURCE

A thin wire is a good approximation to a line heat source. This section shows that with a line source, as in Fig. 1(a), the ratio of temperature oscillation amplitude measured at two points, equal distances upstream and downstream from the source, is pressure self-compensated as a function of the mass flow of a gas.

Let the fluid velocity normal to the line be $u\hat{\mathbf{x}}$, and let the source's oscillatory power dissipation (per unit length) be $W\cos(\omega t)$. By symmetry, $T(\mathbf{r}, \omega)$ depends only on the coordinates x and y where y is in the direction normal to both $\hat{\mathbf{x}}$ and the source. The (x, y) origin is chosen to be the line source. Away from the source, $T(\mathbf{r}, \omega)$ obeys the equation

$$\alpha\left(\frac{\partial^2 T}{\partial x^2} + \frac{\partial^2 T}{\partial y^2}\right) = i\omega T + u\frac{\partial T}{\partial x}. \tag{13}$$

The solution is derived in Appendix B. It can be written

$$T(x, y, \omega) = \frac{W}{2\pi\kappa}\exp\left(\frac{Pe\, x}{2L_0}\right)K_0(rb) \tag{14}$$

where K_0 is a zero order associated Bessel function, $r = \sqrt{(x^2+y^2)}$, and b and L_0 are as in equation (8).

The symmetry of equation (10) for heat waves from a plane source is also found with a line source. In equation (14) it is apparent that

$$\frac{T(x, y, \omega)}{T(-x, y, \omega)} = \exp(Pe\, x/L_0). \tag{15}$$

The phase of $T(\mathbf{r}, \omega)$ depends only on r. Not only is u_p the same in the upstream and downstream directions (at a given r) but also in any other direction from the source.

Consider a gas flow sensor like that in Fig. 1(a) that detects the heat wave amplitude at equal distances upstream and downstream from a line source, and outputs the ratio of the two signals. Since the ratio depends on flow and pressure only through Pe, the sensor responds only to mass flow and is exactly compensated for change in p.

In the limit of very low flow, with constant input power, natural convection is important and the present theory does not apply. Natural convection effects can be identified experimentally by their non-linear dependence on input power. For horizontal wires the onset of natural convection with decreasing flow has been studied experimentally [46].

An actual air flow sensor like that in Fig. 1(a), based on freely suspended hot wires, was reported by Kielbasa and co-workers [15], although they did not investigate the effect of p change. Unfortunately, the maximum flow that could be measured was small. The maximum was set by loss of signal amplitude in the upstream direction with increasing flow, an effect that increases with distance between source and detector. With wires separated by 100 μm the sensor operated in air flows up to about 2 m s^{-1}.

There are two ways to extend the flow range of Kielbasa's sensor: bring the source and detector closer together or put the sensor in a region where $u \ll \bar{u}$. A sensor on the wall uses both strategies. At the wall the flow velocity is zero. A sensor on the wall responds to flow near the surface (in the boundary layer).

5. AUTOMOTIVE AIR FLOW SENSOR MODEL

The air flow sensor that motivated the present study is shown in Fig. 2. It is used to measure air flow into an engine to control the air-to-fuel ratio. The substrate is a silicon wafer coated with polyimide. As discussed in ref. [1] the optimum polyimide thickness is about 15 μm. Polyimide is a good thermal insulator. Silicon is a good thermal conductor. The polyimide layer isolates the heat waves from the silicon so a significant fraction of the detected signal comes through the air. In the automotive application the sensor is mounted in an 8 cm diameter duct and measures flow velocities up to about 60 m s^{-1}.

The automotive sensor is more complicated than the situations discussed in Sections 3 and 4. Here there is a boundary layer and the heat flows in both the substrate and the air; it is no longer true that thermal wave fronts arrive simultaneously at the upstream and downstream points. In fact, comparison of arrival time is one way to measure flow: see Fig. 2(a). Another way is to compare amplitude at the upstream and downstream points as in Sections 3 and 4. The time difference method and the amplitude method are closely related. Both are considered in this section.

The notation used to describe the device is shown in Fig. 2(b). A thin film resistor of width a is used as

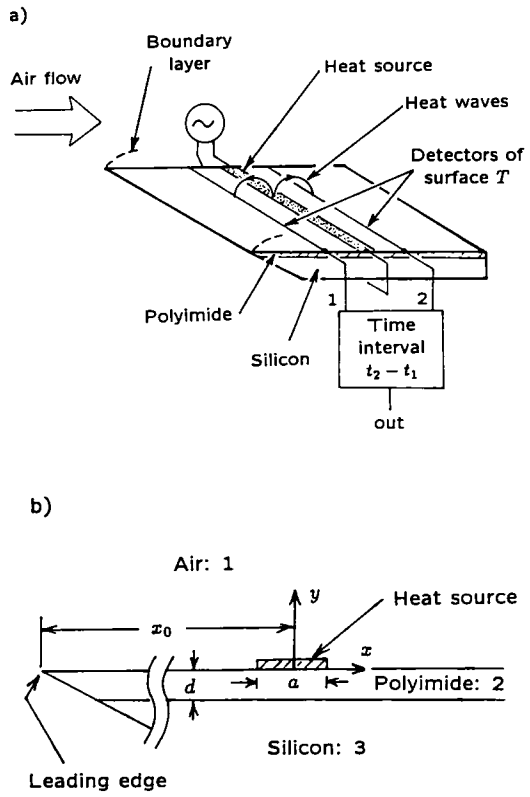

FIG. 2. (a) Schematic diagram of an automotive air flow sensor that compares the propagation time of heat waves moving upstream and downstream along a surface. The heat source is ac through a thin film resistor. Temperature detectors are equally spaced upstream and downstream from the source. The time delay of one signal vs the other is the output. The sensor's output indicates both the magnitude and direction of the flow. (b) Side view showing the notation used in the model. The drawing is not to scale.

the heat source. The polyimide thickness is d. The distance from the leading edge to the heat source is x_0. The drawing is not to scale: typically the heat source is 0.5 μm thick, the polyimide 15 μm thick, the silicon wafer 0.5 mm thick, and x_0 is several mm. The thermal conductivity κ and thermal diffusivity α are labeled by subscripts 1, 2, and 3, in air, polyimide, and silicon, respectively.

The present model is two-dimensional and assumes that temperature is continuous across interfaces [1]. Only at a source is there non-zero total heat flux from an interface. The thickness of the silicon substrate is taken to be infinite. This simplifies the description and introduces no significant loss of accuracy. Typical values of the parameters are listed in Table 1, including the measured α and κ of air [47, 48], silicon [49, 50], and the polyimide [51] used in the sensor.

To solve for the sensor's flow response, three approaches are used. In logical order they are: first, in the limit of low flow (small Pe), an *exact* solution for $T(\mathbf{r}, \omega)$ is obtained with perturbation theory. Heat losses to the substrate and heat exchange with the air are fully accounted for. It assumes that the flow velocity is parallel to the surface and small, but no other assumptions are made—it uses the actual velocity profile in the boundary layer. Second, to validate the perturbation solution and investigate its breakdown as velocity increases, an *exact* solution is obtained with slug flow (velocity independent of distance y from the surface) that is valid at any velocity. If there were complete slip, the slug flow solution would be exact. And third, with flow velocity too large for the direct use of perturbation theory, $T(\mathbf{r}, \omega)$ is approximated by a combination of the perturbation and slug flow solutions.

Since the perturbation solution is based on the exact solution with zero flow velocity—a special case of the slug flow solution—slug flow is discussed first.

In all three situations $T(\mathbf{r}, \omega)$ obeys equation (13) with the appropriate α and flow velocity $u(y)$ in air, polyimide, and the silicon substrate. The boundary conditions are that $T(\mathbf{r}, t)$ is continuous across both interfaces, $|T| \to 0$ as $r \to \infty$, and that heat flux is continuous everywhere except at the source. The heat source is at the air–polyimide interface. It is a strip of width a in which the oscillatory heat dissipation per unit length is $W \cos(\omega t)$. The oscillatory temperature at the detector is derived in Appendix C. On the wall, at position $x\hat{\mathbf{x}}$ relative to the center of the source, and with slug flow $\beta\hat{\mathbf{x}}$, $T(\mathbf{r}, \omega) = T(x, 0, \omega, \beta)$ is given by equation (C6).

Flow affects both the amplitude and phase of detected heat waves. The phase lag at x relative to the oscillation of source power is $-\arg[T(x, 0, \omega, \beta)]$. The corresponding time delay is

$$\tau = -\arg[T(x, 0, \omega, \beta)]/\omega. \tag{16}$$

In Fig. 3 both $\tau(\beta)$ and $|T|(\beta)$ are shown for the situation of Table 1. The integral in equation (C6) was evaluated numerically with IMSL routines DQDAWO and DQAWF [52].

The perturbation solution for $T(\mathbf{r}, \omega)$ with a given $u(y)$ is discussed next. The effect of convection on $T(\mathbf{r}, \omega)$ is the same as if a new heat source was added to the zero flow situation. With distributed heat source $H(\mathbf{r})\exp(i\omega t)$ and steady flow $u(y)\hat{\mathbf{x}}$, the complex temperature field $T(\mathbf{r}, \omega)$ obeys

$$i\omega T + u(y)\hat{\mathbf{x}} \cdot \nabla T = \alpha \nabla^2 T + \alpha H/\kappa. \tag{17}$$

Let $T_a(\mathbf{r}, \omega)$ be the exact solution with no flow. Consider the family of velocity distributions $\varepsilon u(y)$, where $0 \leqslant \varepsilon \leqslant 1$, that give rise to solutions $T_\varepsilon(\mathbf{r}, \omega)$. For small ε

$$T_\varepsilon(\mathbf{r}, \omega) = T_a(\mathbf{r}, \omega) + \varepsilon T_I(\mathbf{r}, \omega) + \varepsilon^2 T_{II}(\mathbf{r}, \omega) + \cdots. \tag{18}$$

The first term in this series, $T_a(\mathbf{r}, \omega)$, is given by equation (C7). As shown in Appendix D, at $y = 0$ the second term is

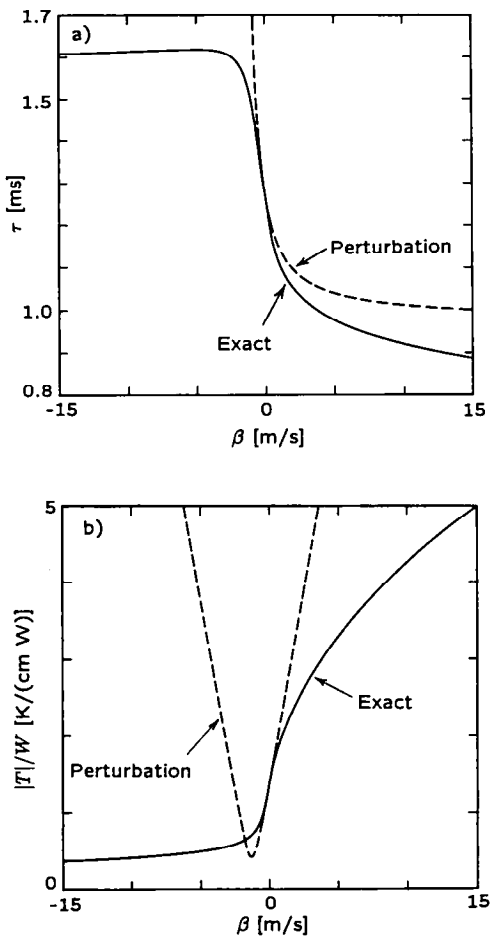

FIG. 3. Comparison between the exact solution and the perturbation solution, both with slug flow. The flow velocity is β. See Table 1 for the situation. In (a) τ is the delay time of signal oscillations relative to the source. In (b) $|T|/W$ is the signal oscillation amplitude normalized by the oscillation amplitude of source power dissipated per unit length.

$$T_1(x,0,\omega) = \int_0^\infty u(y)\Lambda(x,y)\,dy \qquad (19)$$

where $\Lambda(\mathbf{r})$ is given by equation (D7).

The complex valued $\Lambda(x, y)$ gives the linear temperature response at x on the surface to air flow at height y above the surface. A plot of $|\Lambda|$ vs y for the situation of Table 1 is shown in Fig. 4(a). Note that $|\Lambda|$ does not simply decrease exponentially with distance from the wall. There is a maximum at about 11 μm above the surface.

The perturbation solution for $T(\mathbf{r}, \omega)$ is obtained by truncating the series in equation (18) after the T_1 term. The validity of the perturbation solution is tested in Fig. 3 by comparison with the exact solution for slug flow. The first-order approximation is asymptotic with the exact solution at $\beta = 0$ but breaks down at large flow: $|T|$ deviates from the exact solution by 10% at ± 0.5 m s^{-1}. As expected, it breaks down at $\beta \sim u_0 = 0.2$ m s^{-1}.

A better approximation is to use the perturbation solution to find the slug flow that, weighted by Λ, best approximates the actual $u(y)$

$$\beta(u(y)) = \mathrm{Re}\left[\frac{\int_0^\infty u(y)\Lambda(x,y)\,dy}{\int_0^\infty \Lambda(x,y)\,dy}\right]. \qquad (20)$$

Sensor response is calculated by using the slug flow model with this β.

The approximation involved in the use of β from equation (20) comes from the replacement of the actual $u(y)$ in the boundary layer, which is approximately linear near the wall, by an equivalent slug flow that has no shear. Taylor dispersion [35–39] is neglected. A more accurate approach would be to use the analytic solution with $u(y) \propto y$ as the basis for approximation, but that involves the use of special functions of complex argument that are difficult to evaluate [40, 53].

6. FLOW AND PRESSURE RESPONSE

In this Section, the model developed in Section 5 is used to investigate the automotive sensor's flow response and check how closely it approximates an ideal mass flow sensor.

The situation is that of Table 1, as shown in Fig. 2. The heat source is on a flat plate, parallel to the leading edge, at distance x_0 downstream. Laminar flow is incident parallel to the plate.

The sensor responds to flow near the surface. As discussed in Section 2, I_m through a duct that contains the sensor is a function of u_∞ outside the boundary layer and of the air pressure p. Near the surface there is a boundary layer so $u(y) \propto y$ at small y. The Blasius solution is $u(y) = u_\infty f'(\eta)$ where $\eta = y\sqrt{(u_\infty/(\nu x_0))}$. Here f' is the numerical solution to Blasius' ordinary differential equation [54] and ν is air's kinematic viscosity [48, 55].

To obtain the sensor's flow response, the first step is to use equation (20) to calculate $\beta(u_\infty)$, as plotted in Fig. 4(b). The situation is that of Table 1. The functional form of β vs u_∞ is explained as follows. The range of y where Λ is significant is shown in Fig. 4(a). As long as $u(y)$ is approximately linear with y in this range then $\beta \propto u'(0)$ where $u'(0) = du/dy$ at the wall. For the Blasius boundary layer, $u'(0) \propto u_\infty^{3/2}$. Consequently, for small u_∞, $\beta \propto u_\infty^{3/2}$. Actually, this relation is accurate to 8% over the entire range of u_∞ in Fig. 4(b). At large u_∞ this relation must break down since $\beta < u_\infty$.

The sensor in Fig. 2(a) compares the arrival time of wave fronts at detectors upstream and downstream from the heat source. It measures

$$\Delta\tau = \tau(-x) - \tau(x). \qquad (21)$$

With slug flow, τ at the upstream position $-x$ and at

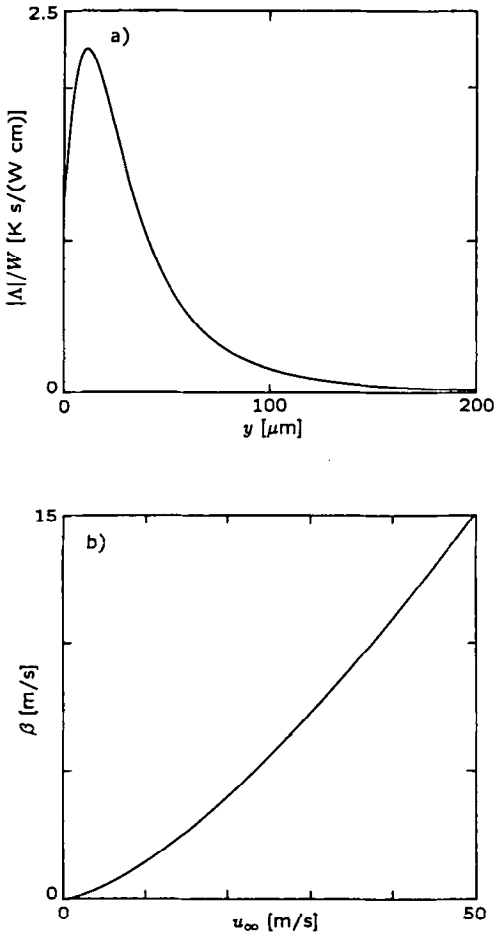

FIG. 4. (a) Plot showing how the sensor responds to a thin jet of air parallel to the surface, at distance y above it. Here Λ is the first-order effect of flow at y on detected signal and W is the source power dissipated per unit length. See Table 1 for the situation. (b) Plot of effective slug flow velocity β vs u_∞, the flow velocity outside the boundary layer. The air flow is incident parallel to a thin flat plate (Blasius boundary layer).

the downstream position x are related by $T(x, 0, \omega, \beta) = T(-x, 0, \omega, -\beta)$. To obtain $\Delta\tau(u_\infty)$, the exact $\tau(x, \beta)$ for slug flow from Fig. 3(a) is evaluated at $\pm\beta(u_\infty)$ from Fig. 4(b). The result is plotted in Fig. 5(a). If the sensor is symmetric, x_0 is the same if the flow reverses and $\Delta\tau(-u_\infty) = -\Delta\tau(u_\infty)$. The sensor indicates both the direction and magnitude of the flow.

A device like that in Fig. 2(a) could respond to heat wave amplitudes at the two detectors instead of arrival time differences. A sensor like those of Sections 3 and 4 would output the ratio

$$\chi = |T(x, 0, \omega)/T(-x, 0, \omega)|. \tag{22}$$

A plot of $\chi(u_\infty)$ obtained by evaluating $|T|(\beta)$ from Fig. 3(b) at $\pm\beta(u_\infty)$ is shown in Fig. 5(b). Note that $\Delta\tau$ saturates at large flow while χ does not.

In experiments, data of $\Delta\tau$ vs u_∞ is consistent with the model, but data of χ vs u_∞ deviates from the model

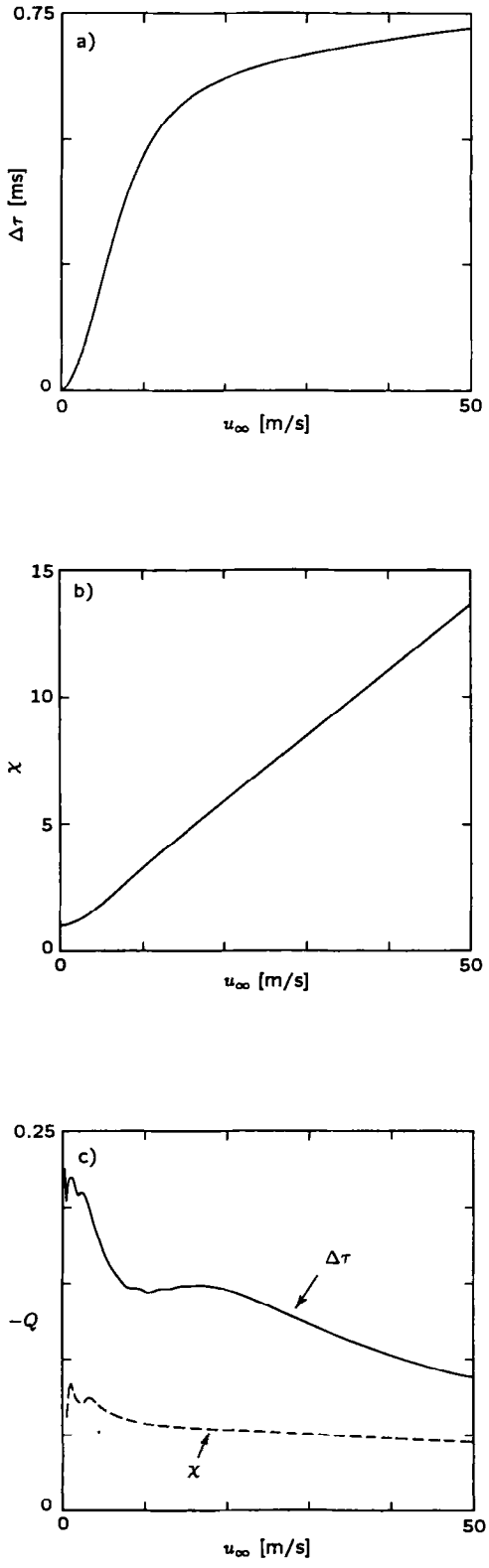

FIG. 5. Response of the automotive air flow sensor. In (a) $\Delta\tau$ is the time delay between the upstream and downstream detectors. In (b) χ is the ratio of the amplitudes measured by the upstream and downstream detectors. In (c) Q is the fractional effect of pressure change (at constant mass flow) on the flow response in (a) and (b). The mass flow (which depends on duct size) is indicated by the flow velocity u_∞ at $p = 100$ kPa. Since $Q < 0$, $-Q$ is plotted.

at large flow—actually χ does saturate like $\Delta\tau$. It is likely that the neglect of Taylor dispersion is responsible for the error in predicted χ. By analogy to the convection–diffusion of heat pulses, Taylor dispersion would be expected to have little effect on $\Delta\tau$ since it has no effect on the average speed at which a pulse moves downstream. Taylor dispersion does, however, cause a pulse to broaden, and this affects χ.

In the automotive application it is important that the sensor's response to mass air flow I_m be insensitive to air pressure p. Let $R(I_m, p)$ be the sensor's output at fixed I_m and p. At fixed p, the I_m indicated by the sensor is the inverse function $R^{-1}(R, p)$, which is independent of p if the sensor responds only to mass flow. A mass flow sensor does not measure p, so if R^{-1} depends on p, and p changes, the measured I_m will be different from the actual I_m. Let ΔI_m be the change in measured I_m (with I_m held constant) caused by a change Δp in p. If Δp is small, then $\Delta I_m \propto \Delta p$. The effect of p on the sensor's response is described by the dimensionless ratio

$$Q(I_m) = \frac{(\Delta I_m/I_m)}{(\Delta p/p)} = \frac{p}{I_m}\frac{\partial R^{-1}}{\partial p}\bigg|_{I_m} = \frac{p}{I_m}\left(\frac{\partial R}{\partial p}\bigg|_{I_m}\right)\left(\frac{\partial R}{\partial I_m}\bigg|_{p}\right)^{-1}. \quad (23)$$

An ideal mass air flow sensor ($R = u_\infty \rho$ is an example) has $Q = 0$. A velocity sensor with $R = \bar{u}$ has $Q(I_m) = -1$.

As shown in Fig. 5(c), Q vs I_m has been calculated for both the $\Delta\tau$ and χ versions of the automotive flow sensor. The model is the same as for Figs. 5(a) and (b). Change of p at constant I_m affects α_1, ν, and u_∞. In Fig. 5(c) the Q oscillations at small I_m are artifacts of the finite difference calculation. A more careful analysis shows that Q approaches a constant as $I_m \to 0$. At small I_m the $\Delta\tau$ and χ curves in Fig. 5(c) should approach $Q = 0.23$ and 0.12, respectively.

7. SUMMARY

Two examples have been given of sensors that use heat waves to measure the mass flow of a gas with exact self-compensation for pressure change: one with a plane heat source, and one with a line heat source. These sensors are limited in size in the flow direction by the need to measure heat waves that move upstream. In them, phase fronts of the heat wave arrive simultaneously at points equal distance upstream and downstream from the source.

Mass flow sensors based on heat waves are conceptually different from mass flow sensors based on average heat transfer. Mass flow sensors based on heat waves must use upstream and downstream propagation distances that are equal and of limited size. Mass flow sensors based on average heat transfer do not have to be small.

In the more realistic situation of an automotive air flow sensor, with source and detectors on a solid substrate, and a boundary layer, pressure self-compensation is no longer exact. The phase arrival symmetry is also broken, so the flow rate can be determined either from the ratio of upstream/downstream amplitude or from the difference in phase arrival times. In Section 6, both are shown to more accurately measure mass flow in a situation of unknown pressure than would a velocity sensor (without pressure information). For example, in the limit of low flow where perturbation theory is accurate, in the 85–100 kPa pressure range, the heat wave sensor that used phase arrival time or amplitude ratio would, respectively, indicate mass air flow with $\pm 1.7\%$ or $\pm 0.9\%$ relative error. A sensor that measured flow velocity would have $\pm 7.5\%$ relative error (independent of flow) in the same pressure range.

The present computational model for the automotive air flow sensor combines perturbation theory with the exact solution for slug flow. The model indicates that the relative error in measured I_m caused by pressure change is largest in the limit of low flow where perturbation theory is valid. The model also shows that the sensor only responds to flow close to the surface, well inside the boundary layer. The present approach is different from that used in ref. [1] to explain the effect of flow on the time-of-flight of heat waves. There it was assumed that the phase velocity u_p of a heat wave in moving fluid is simply $u_p = u + u_0$ where u_0 is the phase velocity in still air and u is the fluid velocity. As shown in Fig. 1(b), that approximation is correct in the downstream direction if $u \gg u_0$, but not in general. One way to improve the present computational model would be to base it on an exact heat wave solution with flow velocity $u(y) \propto y$ instead of slug flow. The use of slug flow neglects Taylor dispersion.

Acknowledgements—I would like to acknowledge the help of E. J. Bissett in addressing the models. I would also like to acknowledge stimulating discussions with J. C. Erskine, C. R. Harrington, R. E. Mayle, and P. C. Wayner, Jr. In particular, Mayle and Wayner, of Rensselaer Polytechnic Institute, used slug flow to model the automotive air flow sensor in unpublished work prepared for and sponsored by General Motors Research Laboratories.

REFERENCES

1. D. K. Lambert and C. R. Harrington, An air flow sensor based on interface thermal wave propagation, *J. Appl. Phys.* **59**, 59–65 (1985). Equation (C7) in the present work corrects a missing factor 2 in the prefactor of equation (9) of this reference.
2. A. F. P. Van Putten and S. Middelhoek, Integrated silicon anemometer, *Electr. Lett.* **10**, 425–426 (1974).
3. J. H. Huijsing, J. P. Schuddemat and W. Verhoef, Monolithic integrated direction-sensitive flow sensor, *IEEE Trans. Electron Devices* **ED-29**, 133–136 (1982).
4. A. F. P. Van Putten, An integrated silicon double bridge anemometer, *Sensors Actuators* **4**, 387–396 (1983).

5. Y. C. Tai, R. S. Muller and R. T. Howe, Polysilicon-bridges for anemometer applications. In *Transducers '85*, pp. 354–357. IEEE (1985).
6. O. Tabata, Fast-response silicon flow sensor with an on-chip fluid temperature sensing element, *IEEE Trans. Electron Devices* **ED-33,** 361–365 (1986).
7. G. N. Stemme, A monolithic gas flow sensor with polyimide as thermal insulator, *IEEE Trans. Electron. Devices* **ED-33,** 1470–1474 (1986).
8. R. G. Johnson and R. E. Higashi, A highly sensitive silicon chip microtransducer for air flow and differential pressure sensing applications, *Sensors Actuators* **11,** 63–72 (1987).
9. N. Tanaka, A. Jinda, J. Tanaka, Y. Inami and M. Hijikigawa, Micro-chip flow sensor for measurement of flow velocity and direction. In *Transducers '87*, pp. 352–355. Institute of Electrical Engineers of Japan (1987).
10. B. W. Van Oudheusden and J. H. Huijsing, Integrated silicon flow-direction sensor, *Sensors Actuators* **16,** 109–119 (1989).
11. B. W. Van Oudheusden, The behavior of a thermal-gradient sensor in laminar and turbulent shear flow, *J. Phys. E* **22,** 490–498 (1989).
12. B. W. Van Oudheusden, Silicon thermal flow sensor with a two-dimensional direction sensitivity, *Meas. Sci. Techn.* **1,** 565–575 (1990).
13. C. H. Stephan and M. Zanini, A micromachined, silicon mass-air-flow sensor for automotive applications. In *Transducers '91*, pp. 30–33. IEEE (1991).
14. J. Kielbasa, J. Rysz, A. Z. Smolarski and B. Stasici, The oscillatory anemometer. In *Fluid Dynamic Measurements in the Industrial and Medical Environments: Proceedings of the Disa Conference* (Edited by D. J. Cockrell), pp. 65–68. Leicester University Press, Old Woking, Surrey, England (1972).
15. J. Kielbasa, J. Piwowarczyk, J. Rysz, A. Z. Smolarski and B. Stasicki, Heat waves in flow metrology. In *Flow Measurement of Fluids* (Edited by H. H. Dijstelbergen and E. A. Spencer), pp. 403–407. North-Holland, Amsterdam (1978).
16. J. Kielbasa, Determination of the flow velocity vector by using the method of heat waves, *Bull. Acad. Pol. Sci.* **26,** 283–289 (1978).
17. L. S. G. Kovásznay, Hot-wire investigation of the wake behind cylinders at low Reynolds numbers, *Proc. R. Soc. Lond. A* **198,** 174–190 (1949).
18. R. E. Walker and A. A. Westenberg, Absolute low speed anemometer, *Rev. Sci. Instrum.* **27,** 844–848 (1956).
19. H. Rahnamai and J. N. Zemel, Pyroelectric anemometers: preparation and flow velocity measurements, *Sensors Actuators* **2,** 3–16 (1981/82).
20. J. R. Frederick, J. N. Zemel and N. Goldfine, Pyroelectric anemometers: experimental geometric considerations, *J. Appl. Phys.* **57,** 4936–4943 (1985).
21. P. Hesketh, B. Gebhart and J. N. Zemel, Heat transfer model for the pyroelectric anemometer, *J. Appl. Phys.* **57,** 4944–4949 (1985).
22. P. I. Geshev, Heat-wave method for studying the structure of a viscous boundary layer, *Teplofiz. Vys. Temp.* **25,** 130–134 (1987) [*High Temp. (USSR)* **25,** 117–121 (1987)].
23. C. Yang, M. Kümmel and H. Søeberg, A transit-time flow meter for measuring milliliter per minute liquid flow, *Rev. Sci. Instrum.* **59,** 314–317 (1988).
24. H. Y. Hsieh, A. Spetz and J. N. Zemel, Wide range pyroelectric anemometers for gas flow measurements. In *Transducers '91*, pp. 38–40. IEEE (1991).
25. A. A. Townsend, The diffusion of heat spots in isotropic turbulence, *Proc. R. Soc. Lond. A* **209,** 418–430 (1951).
26. A. B. Bauer, Direct measurement of velocity by hot-wire anemometry, *AIAA J.* **3,** 1189–1191 (1965).
27. L. J. S. Bradbury and I. P. Castro, A pulsed-wire technique for velocity measurements in highly turbulent flows, *J. Fluid Mech.* **49,** 657–691 (1971).
28. I. H. Tombach, An evaluation of the heat pulse anemometer for velocity measurement in inhomogenous turbulent flow, *Rev. Sci. Instrum.* **44,** 141–148 (1973).
29. J. K. Eaton, R. V. Westphal and J. P. Johnston, Two new instruments for flow direction and skin-friction measurements in separated flows, *ISA Trans.* **21,** 69–78 (1982).
30. H. Sontag and A. C. Tam, Time-resolved flow-velocity and concentration measurements using a traveling thermal lens, *Opt. Lett.* **10,** 436–438 (1985).
31. J. A. Sell, Fluid velocimetry using the photothermal deflection effect. In *Photothermal Investigations of Solids and Fluids* (Edited by J. A. Sell), pp. 213–248. Academic, San Diego (1989).
32. P. M. Handford and P. Bradshaw, The pulsed-wire anemometer, *Exp. Fluids* **7,** 125–132 (1989).
33. W. J. Devenport, G. P. Evans and E. P. Sutton, A traversing pulsed-wire probe for velocity measurements near a wall, *Exp. Fluids* **8,** 336–342 (1990).
34. I. P. Castro and M. Dianat, Pulsed wire velocity anemometry near walls, *Exp. Fluids* **8,** 343–352 (1990).
35. G. Taylor, Dispersion of soluble matter in solvent flowing slowly through a tube, *Proc. R. Soc. Lond. A* **219,** 186–203 (1953).
36. R. Aris, On the dispersion of a solute in a fluid flowing through a tube, *Proc. R. Soc. Lond. A* **235,** 67–77 (1956).
37. W. N. Gill and R. Sankarasubramanian, Dispersion of a non-uniform slug in time-dependent flow, *Proc. R. Soc. Lond. A* **322,** 101–117 (1971).
38. R. Smith, Shear dispersion looked at from a new angle, *J. Fluid Mech.* **182,** 447–466 (1987).
39. I. Frankel and H. Brenner, On the foundations of generalized Taylor dispersion theory, *J. Fluid Mech.* **204,** 97–119 (1989).
40. J. L. Neuringer, Green's function for an instantaneous line particle source diffusing in a gravitational field and under the influence of a linear shear wind, *SIAM J. Appl. Math.* **16,** 834–842 (1968).
41. G. F. Carrier, Useful approximations in Wiener–Hopf problems, *J. Appl. Phys.* **30,** 1769–1774 (1959).
42. H. K. Kuiken, On the influence of longitudinal diffusion in time-dependent convective–diffusive systems, *J. Fluid Mech.* **165,** 147–162 (1986).
43. H. Schlichting, *Boundary-layer Theory* (6th Edn), pp. 258–263. McGraw-Hill, New York (1968).
44. R. F. Blackwelder, Hot-wire and hot-film anemometers. In *Fluid Dynamics* (Edited by R. J. Emrich), Part A, pp. 259–314. Academic, New York (1981).
45. A. E. Perry, *Hot-wire Anemometry*. Oxford, U.K. (1982).
46. D. C. Collis and M. J. Williams, Two-dimensional convection from heated wires at low Reynolds numbers, *J. Fluid Mech.* **6,** 357–384 (1959).
47. Y. S. Touloukian, P. E. Liley and S. C. Saxena, *Thermophysical Properties of Matter*. Vol. 3, p. 512. Plenum, New York (1970).
48. D. R. Lide, *CRC Handbook of Chemistry and Physics* (71st Edn), Section 6, p. 1. CRC Press, Boca Raton, Florida (1991).
49. Y. S. Touloukian, R. W. Powell, C. Y. Ho and P. G. Klemens, *Thermophysical Properties of Matter*. Vol. 1, p. 339. Plenum, New York (1970).
50. Y. S. Touloukian, R. W. Powell, C. Y. Ho and M. C. Nicolaou, *Thermophysical Properties of Matter*. Vol. 10, p. 160. Plenum, New York (1973).
51. D. K. Lambert, Polyimide film on silicon: use of IR emission modulation to obtain thermal conductivity. In *Thermal Conductivity 21* (Edited by C. J. Cremers and H. A. Fine). pp. 209–221. Plenum, New York (1990).
52. R. Piessens, E. de Doncker-Kapenga, C. W. Überhuber and D. K. Kahaner, *QUADPACK: A Subroutine Package for Automatic Integration*. Springer, Berlin (1983).
53. M. Soliman and P. L. Chambré, On the time-dependent Lévêque problem, *Int. J. Heat Mass Transfer* **10,** 169–180 (1967).

54. L. Howarth, On the solution of the laminar boundary layer equations, *Proc. R. Soc. Lond. A* **164**, 547–579 (1938).
55. Y. S. Touloukian, S. C. Saxena and P. Hestermans, *Thermophysical Properties of Matter*. Vol. 11, p. 611. Plenum, New York (1975).
56. To obtain equation (B8) a change of variables was used to transform the integral into the cosine transform given as 1.4 (27) in H. Bateman, *Tables of Integral Transforms*, Vol. 1, p. 17. McGraw-Hill, New York (1954).
57. G. Barton, *Elements of Green's Functions and Propagation*, p. 206. Oxford, U.K. (1989).

APPENDIX A: PLANE SOURCE

A solution to equation (6) is

$$T(x,\omega) = C\exp(\xi x), \tag{A1}$$

provided that $\alpha\xi^2 - u\xi - i\omega = 0$. The two complex ξ roots correspond to plane heat waves moving upstream and downstream. The waves are assumed to originate at $x = 0$, so solutions that grow as $|x| \to \infty$ are unphysical: in the region with $x < 0$ the solution must use the root with $\mathrm{Re}(\xi) \geqslant 0$, and in the region with $x > 0$ the solution must use the root with $\mathrm{Re}(\xi) \leqslant 0$. Explicitly, for $u \geqslant 0$

$$\xi = \frac{u}{2\alpha} - \frac{x}{|x|}b \tag{A2}$$

where b is the root with positive real part given by equation (9).

The boundary conditions in equation (7) between T_+ with $x > 0$ and T_- with $x < 0$ determine their prefactors. The final result for $u \geqslant 0$ is

$$T(x,\omega) = \frac{W}{2\kappa b}\exp\left(\frac{ux}{2\alpha} - |x|b\right). \tag{A3}$$

APPENDIX B: LINE SOURCE

To find $T(\mathbf{r}, \omega)$ that solves equation (13), with a line heat source at $\mathbf{r} = 0$, it is convenient to divide the space into two regions by the plane with $y = 0$. Let T_+ and T_- be the solutions in the regions with $y > 0$ and $y < 0$, respectively. The boundary conditions are

$$y = 0: \quad T_+ = T_-, \quad -\kappa\frac{\partial T_+}{\partial y} + \kappa\frac{\partial T_-}{\partial y} = W\delta(x). \tag{B1}$$

Equation (13) is converted to an ordinary differential equation by a Fourier transform with respect to x. The Fourier transform and its inverse are

$$T(x,y,\omega) = \frac{1}{\sqrt{(2\pi)}}\int_{-\infty}^{\infty}\tilde{T}(s,y,\omega)e^{isx}\,ds, \tag{B2}$$

$$\tilde{T}(s,y,\omega) = \frac{1}{\sqrt{(2\pi)}}\int_{-\infty}^{\infty}T(x,y,\omega)\,e^{-isx}\,dx. \tag{B3}$$

After Fourier transformation, equation (13) becomes

$$\alpha\left(-s^2\tilde{T} + \frac{d^2\tilde{T}}{dy^2}\right) = i\omega\tilde{T} + isu\tilde{T}. \tag{B4}$$

The boundary conditions become

$$y = 0: \quad \tilde{T}_+ = \tilde{T}_-, \quad -\kappa\frac{\partial\tilde{T}_+}{\partial y} + \kappa\frac{\partial\tilde{T}_-}{\partial y} = \frac{W}{\sqrt{(2\pi)}}. \tag{B5}$$

The solution of equation (B4) is

$$\tilde{T}(s,y,\omega) = C\exp(-m|y|) \tag{B6}$$

where $\mathrm{Re}(m) > 0$ to satisfy the requirement that $|\tilde{T}_\pm| \to 0$ as $|y| \to \infty$. Explicitly, m is the root with positive real part: $m = \sqrt{(s^2 + i(\omega + us)/\alpha)}$. Let C_+ and C_- be the prefactors in equation (B6) for T_+ and T_-, respectively. Equation (B5) implies that

$$C_+ = C_- = W/(2\kappa m\sqrt{(2\pi)}). \tag{B7}$$

The solution for a line heat source is [56]

$$T(x,y,\omega) = \frac{W}{4\pi\kappa}\int_{s=-\infty}^{\infty}\frac{\exp(-m|y| + isx)}{m}\,ds$$

$$= \frac{W}{2\pi\kappa}\exp\left(\frac{ux}{2\alpha}\right)K_0(rb) \tag{B8}$$

where K_0 is a zero-order associated Bessel function, $r = \sqrt{(x^2+y^2)}$, and b is defined in equation (9).

APPENDIX C: SLUG FLOW

With slug flow, the situation is shown in Fig. 2(b). There are three regions: the air is 1, the polyimide is 2, and the silicon substrate is 3. Let T_1, T_2, and T_3 be T in regions 1, 2, and 3, respectively. In each region, T obeys equation (13). With slug flow, $u(y) = \beta$ in region 1, and $u = 0$ in regions 2 and 3. Since the partial differential equations for T are linear, it is convenient to first solve the simpler problem of a line heat source at $\mathbf{r} = 0$ on the interface between regions 1 and 2. The solution with a line source and slug flow is $T_L(\mathbf{r}, \omega)$. The desired $T(\mathbf{r}, \omega)$ with an extended source and slug flow is the convolution of the source with $T_L(\mathbf{r}, \omega)$.

To solve for $T_L(\mathbf{r}, \omega)$, a line source at the air–polyimide interface is included in the boundary conditions

$$y = 0: \quad T_1 = T_2, \quad -\kappa_1\frac{\partial T_1}{\partial y} + \kappa_2\frac{\partial T_2}{\partial y} = W\delta(x);$$

$$y = -d: \quad T_2 = T_3, \quad -\kappa_2\frac{\partial T_2}{\partial y} + \kappa_3\frac{\partial T_3}{\partial y} = 0. \tag{C1}$$

An additional requirement is that $T_L(\mathbf{r}, \omega) \to 0$ as $y \to \pm\infty$.

A Fourier transform with respect to x converts equation (13) into equation (B4). The solution of equation (B4) that has the correct limits as $y \to \pm\infty$ in regions 1 and 3 is

$$\tilde{T}_1(s,y) = C_1 e^{m_1 y}$$

$$\tilde{T}_2(s,y) = C_{2a}e^{m_2 y} + C_{2b}e^{-m_2 y}$$

$$\tilde{T}_3(s,y) = C_3 e^{m_3 y}, \tag{C2}$$

where m_1, m_2, and m_3 are the roots with positive real part: $m_1 = \sqrt{(s^2 + i(\omega + s\beta)/\alpha_1)}$, $m_2 = \sqrt{(s^2 + i\omega/\alpha_2)}$, and $m_3 = \sqrt{(s^2 + i\omega/\alpha_3)}$.

The transformed boundary conditions are

$$y = 0: \quad \tilde{T}_1 = \tilde{T}_2, \quad -\kappa_1\frac{\partial\tilde{T}_1}{\partial y} + \kappa_2\frac{\partial\tilde{T}_2}{\partial y} = \frac{W}{\sqrt{(2\pi)}}$$

$$y = -d: \quad \tilde{T}_2 = \tilde{T}_3, \quad -\kappa_2\frac{\partial\tilde{T}_2}{\partial y} + \kappa_3\frac{\partial\tilde{T}_3}{\partial y} = 0. \tag{C3}$$

The boundary conditions give four equations to solve for the four complex numbers C_1, C_{2a}, C_{2b}, and C_3. The desired $T_L(\mathbf{r}, \omega)$ is equation (C2) with

$$C_1 = \frac{W(M_A + M_B)}{(2\pi)^{1/2}(M_A M_C + M_B M_D)}$$

$$C_{2a} = \frac{WM_A}{(2\pi)^{1/2}(M_A M_C + M_B M_D)}$$

$$C_{2b} = \frac{WM_B}{(2\pi)^{1/2}(M_A M_C + M_B M_D)}$$

$$C_3 = \frac{2W\kappa_2 m_2}{(2\pi)^{1/2}(M_A M_C + M_B M_D)}e^{(m_3 - m_2)d} \tag{C4}$$

where $M_A = \kappa_2 m_2 + \kappa_3 m_3$, $M_B = (\kappa_2 m_2 - \kappa_3 m_3)\,e^{-2m_2 d}$, $M_C = \kappa_1 m_1 + \kappa_2 m_2$, and $M_D = \kappa_1 m_1 - \kappa_2 m_2$.

With an extended source, $T(\mathbf{r}, \omega)$ is the convolution of

$T_L(\mathbf{r}, \omega)$ with the source. The Fourier transform of the convolution of two functions is the product of the two individual Fourier transforms. The result for a source evenly distributed in the $|x| < a/2$ region of the $y = 0$ plane is

$$\tilde{T}(s, y) = \frac{2 \sin (sa/2)}{sa} \tilde{T}_L(s, y). \quad \text{(C5)}$$

On the wall $T(\mathbf{r}, \omega)$ is

$$T(x, 0, \omega) = \frac{W}{\pi a} \int_{-\infty}^{\infty} \frac{(M_A + M_B) \sin (sa/2) e^{isx}}{s(M_A M_C + M_B M_D)} ds. \quad \text{(C6)}$$

In still air equation (C6) simplifies to

$$T_a(x, 0, \omega) = \frac{2W}{\pi a} \int_0^{\infty} \frac{(M_A + M_B) \sin (sa/2) \cos (sx)}{s(M_A M_C + M_B M_D)} ds. \quad \text{(C7)}$$

APPENDIX D: PERTURBATION SOLUTION

In a region without heat sources, to first-order in ε, equations (17) and (18) give

$$i\omega T_1 - \alpha \nabla^2 T_1 = -u(y) \frac{\partial T_a}{\partial x}. \quad \text{(D1)}$$

In equation (D1) T_1 plays the same role as T in equation (17) with still air. In this interpretation the source of T_1 is

$$H_1(\mathbf{r}) = -\frac{\kappa u(y)}{\alpha} \frac{\partial T_a}{\partial x}. \quad \text{(D2)}$$

The solution for $T_1(\mathbf{r}, \omega)$ can be expressed in terms of $T_a(\mathbf{r}, \omega)$ the still air solution derived in Appendix C. The effect of $H_1(\mathbf{r})$ on T_1 is linear so

$$T_1(\mathbf{r}, \omega) = \int H_1(\mathbf{r}') G(\mathbf{r}', \mathbf{r}) \, dA' \quad \text{(D3)}$$

where $G(\mathbf{r}', \mathbf{r})$ is $T(\mathbf{r}, \omega)$ in still air from a fictitious line source of heat at $\mathbf{r}'$, oscillating in phase with the actual source, with unit amplitude.

The detected T_1 is at $\mathbf{y} = 0$. By reciprocation [57], in still air $G(\mathbf{r}', \mathbf{r}) = G(\mathbf{r}, \mathbf{r}')$, so

$$G(x', y', x, 0) = T_L(x' - x, y')/W. \quad \text{(D4)}$$

The perturbation solution in terms of T_L (with $u = 0$) and T_a is

$$T_1(x, 0, \omega) = \frac{-\kappa_1}{\alpha_1 W} \int u(y) \left[\frac{\partial}{\partial x'} T_a(x', y', \omega) \right] \times T_L(x' - x, y', \omega) \, dA'. \quad \text{(D5)}$$

The expressions derived in Appendix C for T_a and T_L are Fourier transforms. It is simpler to evaluate T_1 if it is expressed directly in terms of the Fourier transformed quantities $\tilde{T}_a$ and $\tilde{T}_L$ with still air

$$T_1(x, 0, \omega) = \int_0^{\infty} u(y) \Lambda(x, y) \, dy \quad \text{(D6)}$$

where

$$\Lambda(x, y) = \frac{-i\kappa_1}{\alpha_1 W} \int_{-\infty}^{\infty} s \tilde{T}_a(s, y, \omega) \tilde{T}_L(s, y, \omega) e^{isx} ds$$

$$= \frac{-\kappa_1 W}{\pi \alpha_1 a} \int_{-\infty}^{\infty} \frac{(M_A + M_B)^2}{(M_A M_C + M_B M_D)^2} \times \sin (sa/2) \exp (isx - 2m_1 y) \, ds. \quad \text{(D7)}$$